Structural Engineering and Mechanics, Vol. 9, No. 5 (2000) 491-504
DOI: http://dx.doi.org/10.12989/sem.2000.9.5.491

Retrofitting by adhesive bonding steel plates to the sides of R.C. beams. Part 1: Debonding of plates due to flexure

Deric. J. Oehlers† and Ninh T. Nguyen‡

Department of Civil and Environmental Engineering, University of Adelaide, SA 5050, Australia

Mark A. Bradford†‡

School of Civil Engineering, University of New South Wales, Australia

Abstract. A convenient method for enhancing the strength and stiffness of existing reinforced concrete beams is to bond adhesively steel plates to their tension faces. However, there is a limit to the applicability of tension face plating as the tension face plates are prone to premature debonding and, furthermore, the addition of the plate reduces the ductility of the beam. An alternative approach to tension face plating is to bond adhesively steel plates to the sides of reinforced concrete beams, as side plates are less prone to debonding and can allow the beam to remain ductile. Debonding at the ends of the side plates due to flexural forces, that is flexural peeling, is studied in this paper. A fundamental mathematical model for flexural peeling is developed, which is calibrated experimentally to produce design rules for preventing premature debonding of the plate-ends due to flexural forces. In the companion paper, the effect of shear forces on flexural peeling is quantified to produce design rules that are applied to the strengthening and stiffening of continuous reinforced concrete beams.

Key words: retrofitting; rehabilitation; adhesive bonding; plating; reinforced concrete; flexural peeling.

1. Introduction

Continuos reinforced concrete slabs and beams are frequently strengthened and stiffened by bonding steel plates to their tension faces (Swamy, Jones and Bloxham 1987, Oehlers, Ali and Lou 1998a) as shown in Fig. 1(a). Research has shown that the plate-ends tend to peel away from the reinforced concrete beam and that this peeling mechanism is induced by diagonal shear cracks formed by vertical shear forces which will be referred to as shear peeling (Oehlers 1992), and also depends on the curvature at the plate-end which will be referred to as flexural peeling (Oehlers and Moran 1990). As most slabs do not require stirrups, the applied vertical shear forces, and, therefore, the effect of shear peeling, can be said to be relatively small. It is for this reason that the technique of tension face plating has worked so well for reinforced concrete slabs (Oehlers 1995).

Tension face plating can also be applied to reinforced concrete beams. However as beams

† Senior Lecturer
‡ Former Research Fellow
†‡ Professor

generally require stirrups, the vertical shear forces are relatively large, so that shear peeling that is induced by the formation of diagonal cracks can often cause the tension face plate to debond prematurely. In fact, shear peeling may make it impractical to plate beams by causing debonding before the design load is reached (Oehlers 1992). However, premature debonding of the ends of tension face plates glued to beams can be prevented by adding side plates, as in Fig. 1(b), as the side plates can increase substantially the shear peeling resistance (Oehlers, Ali and Lou 1997). These side plates are always placed adjacent to the plate-ends and over a relatively short length of beam on each side of the plate-end as their sole purpose is to enhance the resistance to shear peeling.

Apart from the problems with shear peeling, it is also worth noting that tension face plates act as additional tension reinforcement and, hence, reduce the ductility of the beam or make it over-reinforced, which may also limit the application of this technique. A natural progression to tension face plating, as shown in Figs. 1(a) and (b), is to only use side plates as in Fig. 1(c), because deep side plates, that is plates which are almost as deep as the reinforced concrete beam or the web of the beam, automatically enhance the shear peeling resistance by acting as the side plates in Fig. 1(b), and can even increase the ductility of the beam (Smith and Bradford 1995), as well as prevent the beam from becoming over-reinforced. Furthermore, side plates can be used in conjunction with tension face plates as in Fig. 1(d) and it is felt that this mixed form of plating will significantly

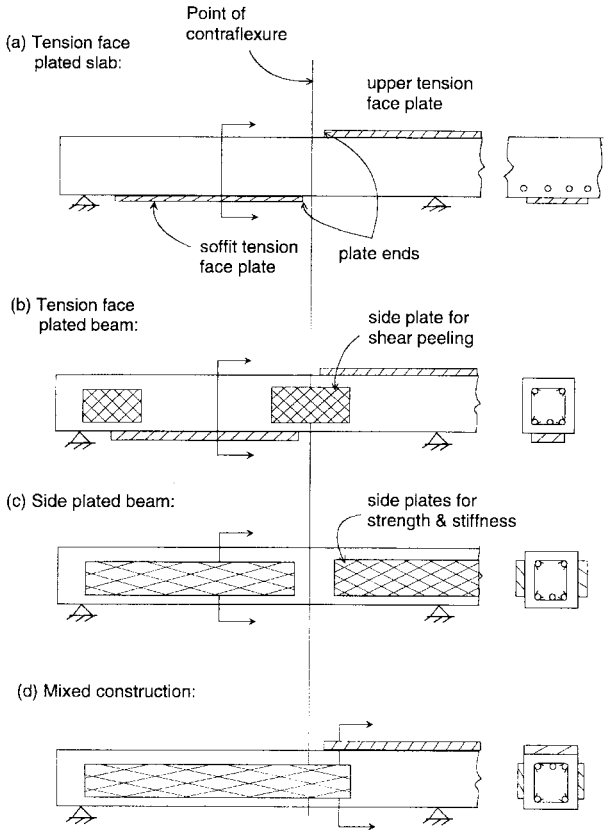

Fig. 1 Types of plating

increase the range of structures to which plating can be applied.

Design rules for preventing premature debonding of the ends of side plates is developed in this paper and the companion paper (Oehlers, Nguyen and Bradford 1998b) and are applied to the strengthening and stiffening of continuous reinforced concrete beams. These design rules can cope with any combination of applied loads, with any combination of beam restraints, with propped and unpropped construction, and can allow for short term loads and the long term time effects of creep and shrinkage. Research on tension face plates (Oehlers and Moran 1990, Oehlers 1992) has quantified debonding due to pure flexure, debonding due to pure shear and the interaction between flexural peeling and shear peeling. A similar strategy has been used to develop design rules for side plated beams. Part 1 of this paper concentrates on debonding due to flexural peeling. A mathematical model for flexural peeling is first developed which is then calibrated from tests and adapted to form a design rule. In the companion paper, design rules for shear peeling and then the interaction between shear peeling and flexural peeling are developed, and applied to both tension face and side plating of reinforced concrete beams.

2. Fundamental mathematical model for flexural peeling

2.1. Debonding stress resultants

The reinforced concrete beam of width b_c in Fig. 2(a) has plates of depth h_p and thickness t_{sp} glued to both sides. The distance between the neutral axis of the composite plated beam, line A-A in Fig. 2(b), and the centroid of the plates, line B-B, is $h_{p,cmp}$. As the plate is glued to the reinforced concrete element, the vertical and longitudinal slip of the plate relative to the reinforced concrete beam is negligible so that the strain distribution is uni-linear as shown, where ϕ is the curvature. In this analysis, it is assumed that the behaviour of the composite beam is linear elastic as we are dealing with the debonding of real structures where the plates are terminated a long way from the position of maximum moment.

Let us assume that the composite beam is subjected to a constant moment of magnitude M_{cmp} as in Fig. 3(a). This moment induces the strain distribution in Fig. 2(b) and, hence, the stress resultants in each of the three elements of the composite beam in Figs. 3(b) and (c), where M_p = the moment in a plate about the centroid of the plate; F_p = axial force in a plate; M_{RC} = moment in the reinforced concrete element about the centroid of the element, and where the axial force in the

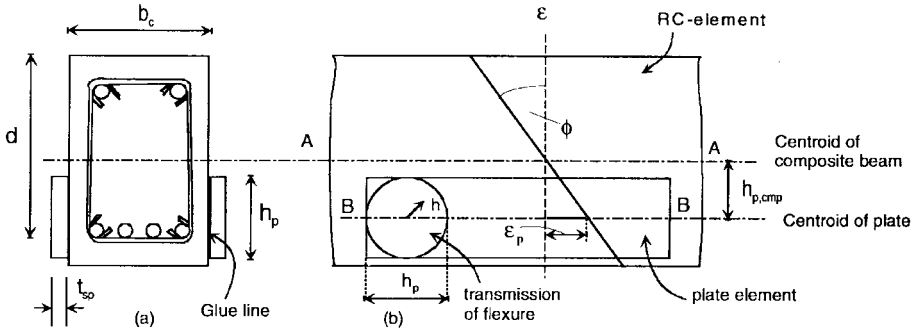

Fig. 2 Composite plated beam

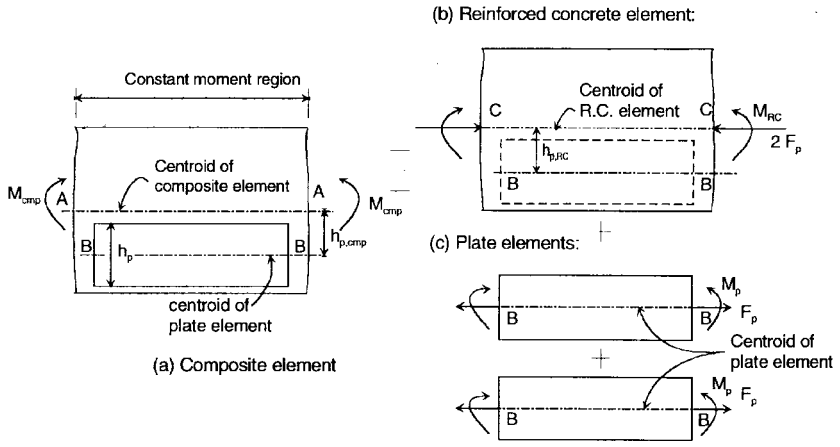

Fig. 3 Free body diagram of plated beam

reinforced concrete element is $2F_p$ as it is in equilibrium with the axial force in both plates; and where the distance between the centroid of the reinforced concrete element and the centroid of the plates is $h_{p,RC}$.

It can be seen in Fig. 3 that the applied moment M_{cmp} induces a moment M_p and axial force F_p in the plate. These stress resultants are transferred from the reinforced concrete element to the plate through stresses at the plate/beam interface and it is these stresses than can cause the plate to debond. In the following section, models are developed for the interface stresses induced by M_p and F_p which are then combined to determine the parameters that control flexural peeling. These parameters are then calibrated through tests to form design rules.

2.1.1. Flexural debonding component M_p

As the plates are glued to the reinforced concrete beam, as in Fig. 2(a), there is no vertical slip between the plate elements and the reinforced concrete element, so that the curvatures in these elements are the same as shown in Fig. 2(b). Therefore, for the moments in Fig. 3

$$\phi=\frac{M_{RC}}{(EI)_{RC}}=\frac{M_p}{(EI)_p}=\frac{M_{cmp}}{(EI)_{cmp}} \tag{1}$$

where $(EI)_{RC}$ = flexural rigidity of the reinforced concrete element; $(EI)_p$ = flexural rigidity of a plate; and $(EI)_{cmp}$ = flexural rigidity of the composite plated beam. Therefore, the moment that can cause debonding of a plate M_p is given by

$$M_p=M_{cmp}\frac{(EI)_p}{(EI)_{cmp}} \tag{2}$$

2.1.2. Axial debonding component F_p

From Fig. 2(b), the strain at the centroid of a plate, ε_p, is given by

$$\varepsilon_p=h_{p,cmp}\phi \tag{3}$$

Therefore,

$$F_p=A_pE_p\varepsilon_p=(EA)_ph_{p,cmp}\phi \tag{4}$$

where E_p=Young's modulus of plate, $A_p=h_p t_{sp}$=area of plate. Substituting for ϕ from Eq. (1) gives the axial force that can cause debonding as

$$F_p=\frac{(EA)_p h_{p,cmp} M_{cmp}}{(EI)_{cmp}} \tag{5}$$

2.2. Transmission of debonding stress resultants

Debonding of the plate-end occurs in an 'elastic' region of a beam, that is well away from the region of maximum moment where non-linear ultimate strength analyses apply. However, the debonding mechanism is extremely complex having to deal with such problems as concrete cracking, aggregate interlock and tension stiffening. Therefore, instead of trying to produce an exact model for this complex problem, the parameters that control the stresses that the debonding stress resultants M_p and F_p induce will be derived. These parameters will then be calibrated experimentally.

2.2.1. Flexural debonding component M_p

Let us assume that the end of the plate of area of $(h_p \times h_p)$ transmits the debonding moment M_p from the reinforced concrete beam into the plate as shown on the left hand side of the plate in Fig. 2(b). The moment M_p is transmitted into the plate through the shear forces acting at the interface between the concrete and side plate. It will be assumed that initial debonding occurs at the corners of the square bonded area, so that eventually M_p is transmitted by shear in the circular bonded area or radius $h=h_p/2$.

As a linear elastic analysis is being applied and from elementary mechanics (Nguyen and Oehlers 1997a), the shear stress τ_h at a distance h from the center of the transmission zone varies linearly and is given by $\tau_h=2h\tau_{max}/h_p$ where τ_{max} is the maximum shear stress at the periphery. Hence, the moment increment due to the shear stress τ_h is $dM=2\pi h\tau_h h dh=4\pi h^3\tau_{max}dh/h_p$. Integrating over the bonded area and substituting for M_p in Eq. (2) gives

$$\tau_{max}=\frac{16M_p}{\pi h_p^3}=\frac{16M_{cmp}(EI)_p}{\pi h_p^3(EI)_{cmp}} \tag{6}$$

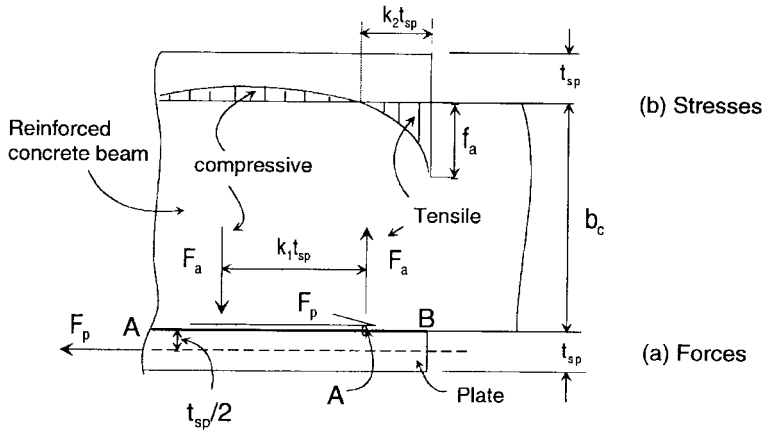

Fig. 4 Transmission of F_p

2.2.2. Axial debonding component F_p

Let us consider how the axial force F_p is transmitted from the reinforced concrete beam to the side plates as shown in the plan view of the plated beam in Fig. 4(a). A shear force F_p acts across the interface A-B and where the plate is uniformly stressed the axial force in the plate F_p acts at an eccentricity $t_{sp}/2$ from the interface as shown. Therefore, the couple $F_p t_{sp}/2$ has to be balanced by the normal forces across the interface F_a which must be tensile adjacent to the plate-end at B and compressive away from the end as shown. As the plate thickness t_{sp} is much less than the width of the beam b_c, it can be assumed that the lever arm between the resultant normal forces is proportional to t_{sp}, that is $k_1 t_{sp}$ as shown. From the equilibrium of the forces acting on the plate element

$$F_a = \frac{F_p}{2k_1} \tag{7}$$

Finite element analyses of the stress distribution across the interface (Oehlers and Moran 1992) are shown adjacent to the top plate in Fig. 4(b). The tensile stresses are concentrated over a short zone of length $k_2 t_{sp}$ which is assumed to be proportional to t_{sp} as $t_{sp} << b_c$, they occur over the depth of the plate h_p, and have a peak value at the plate-end of f_a. If we define the shape of the tensile stress distribution as s_a, where the mean tensile stress is $s_a f_a$, then

$$F_a = (s_a f_a)(k_2 t_{sp}) h_p \tag{8}$$

From Eqs. (7) and (8) and substituting $F_p = f_p t_{sp} h_p$ where $f_p = E_p \varepsilon_p$, gives

$$f_a = (2k_1 k_2 s_a)^{-1} f_p = k_a f_p = k_a E_p \varepsilon_p \tag{9}$$

Substituting Eq. (3) into Eq. (9) and ϕ from Eq. (1) gives the maximum normal stress across the interface as

$$f_a = k_a E_p \phi h_{p,cmp} = k_a E_p \frac{M_{cmp}}{(EI)_{cmp}} h_{p,cmp} \tag{10}$$

which is the stress that causes the plate to debond as in Fig. 9.

2.2.3. Interaction between debonding stresses

We have dealt with both the shear force across the interface A-B in Fig. 4(a) that is induced by M_p and which has a maximum value of τ_{max}, and the normal tensile force across the interface that is induced by F_p and which has a maximum value of f_a. The shear force F_p in Fig. 4(a) also induces a shear stress τ_F. Let us consider the stresses at point A in Fig. 4(a) which lies at the interface and is close to the plate-end at point B. Point A is also shown in Fig. 5(a) and the stresses at the interface are shown in Fig. 5(b) where f_F is the normal tensile stress across the interface induced by F_p, τ_M is the shear stress induced by M_p and τ_{sh} is the shear stress induced by F_p. As point A is moved towards point B, $\tau_M \rightarrow \tau_{max}$, $f_F \rightarrow f_a$, and $\tau_M \rightarrow 0$ as the face C in Fig. 5(b) is a free edge at the plate-end. Therefore, the stress distribution at the plate-end is that shown in Fig. 5(c) which will be used in the following analysis to form the fundamental equation for the debonding of side plates. However, it has been shown (Nguyen and Oehlers 1997a) that the shape of this equation also applies at point A where τ_M exists.

If we assume that debonding occurs when the principal tensile stress in Fig. 5(c) is equal to the tensile strength of the concrete f_t, then from Mohr's stress circle (Ryder 1974).

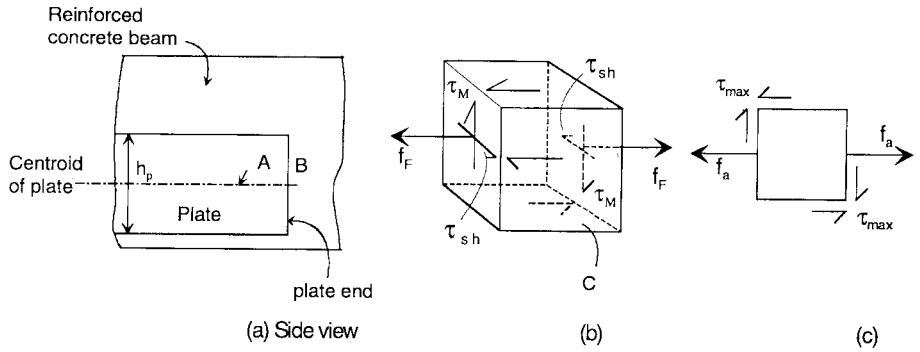

Fig. 5 Debonding stresses

$$0.5f_a+\sqrt{\tau_{\max}^2+(0.5f_a)^2}=f_t \tag{11}$$

The parameter $\sqrt{\tau_{\max}^2+(0.5f_a)^2}$ in Eq. (11) can be written as $k_R\tau_{\max}+0.5f_a$ where $k_R=f(\tau_{\max}, f_a)$. If we assume as a first approximation that k_R is constant, then Eq. (11) becomes

$$f_a+k_R\tau_{\max}=f_t \tag{12}$$

Substituting into Eq. (12), Eqs. (16) and (10) and $I_p=t_{sp}h_p^3/12$ gives

$$k_A+k_B\left(\frac{t_{sp}}{h_{p,cmp}}\right)=\frac{f_t(EI)_{cmp}}{M_{cmp}E_ph_{p,cmp}} \tag{13}$$

Eq. (13) clearly shows the main variables that affect debonding of side plates. The obvious variables are the plate thickness, the tensile strength of the concrete and the applied moment. However, it can also be seen that the flexural rigidity of the composite plated beam is important as well as the distance between the centroid of the plate and that of the composite plated beam.

Eq. (13) can be written as the following linear variation

$$k_A+k_BX=Y \tag{14}$$

where the non-dimensional parameters that control debonding of side plated beams are

$$X=\frac{t_{sp}}{h_{p,cmp}} \tag{15}$$

and

$$Y=\frac{f_t(EI)_{cmp}}{M_{cmp}E_ph_{p,cmp}}=\frac{f_t}{E_p\varepsilon_p} \tag{16}$$

The following experimental program was based on these non-dimensional parameters and designed to determine the coefficients k_A and k_B in Eq. (14).

3. Experimental work

3.1. Specimens

Six 5 m long composite plated beams with the cross-sectional properties in Fig. 6(b) were tested

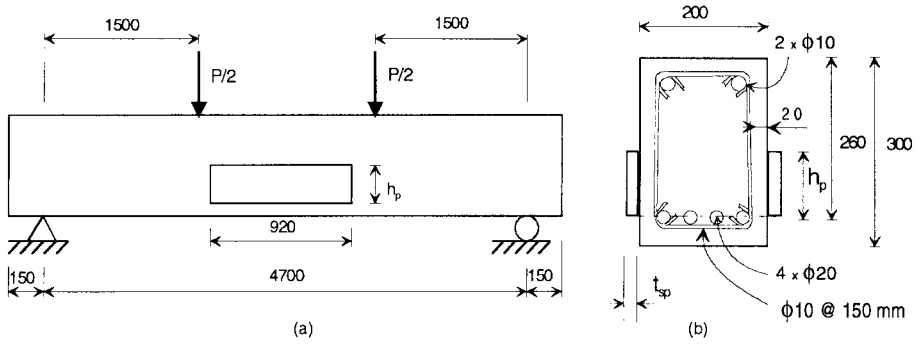

Fig. 6 Specimen and rig

with the plates in a constant moment region as shown in Fig. 6(a). The beams are referred to as 1a to 1f in column 1 in Table 1. The notation N in column 1 refers to the plate on the north side of the beam and S refers to the plate on the south side. The debonding of each plate was treated as a separate test so there are twelve results in all. The plate thickness was varied from 6 to 12 mm as shown in column 2 and the plate depth from 60 to 240 mm as in column 3. The concrete material properties at the time of testing are given in columns 4 for the Young's modulusE_c, in column 5 for the Brazilian tensile strengthf_b, and the average concrete cylinder compressive strengthf_c= 54 N/mm^2 (Nguyen and Oehlers 1997b). The 20 mm diameter reinforcing bars in Fig. 6(b) had a yield strength of 461 N/mm^2 and the yield strengths of the 6, 8 and 12 mm plates were 331, 321 and 289 N/mm^2 respectively. A standard procedure was used for gluing the plates to the beam (Oehlers and Moran 1990) which worked very well as the debonding failure plane always occurred within the concrete. The plates were strain gauged with a typical arrangement shown in Fig. 7. Full details of the composite plated beams and test results are given elsewhere (Nguyen and Oehlers 1997b).

Table 1 Beam specimens and results

	t_{sp}	h_p	E_c	f_b	M_i	M_u	ε_u (10^{-6})	
Tests	(mm)	(mm)	(kN/mm^2)	(MPa)	(kNm)	(kNm)	bottom	top
(1)	(2)	(3)	(4)	(5)	(6)	(7)	(8)	(9)
1aN	8	60	39.8	4.46	18.0	61.0	570	400
1aS	8	60	39.8	4.46	18.0	85.1	828	562
1bN	8	180	39.8	4.47	38.5	85.7	837	-455
1bS	8	180	39.8	4.47	69.5	106.7	1047	-534
1cN	8	210	40.0	4.42	66.2	91.9	894	-721
1cS	8	210	40.0	4.42	63.2	94.8	936	-598
1dN	8	240	39.7	4.50	48.9	90.2	898	-762
1dS	8	240	39.7	4.50	35.5	91.6	885	-792
1eN	6	180	39.7	4.51	37.1	112.9	1082	-777
1eS	6	180	39.7	4.51	56.5	114.3	1183	-530
1fN	12	180	39.6	4.54	28.3	80.3	740	-466
1fS	12	180	39.6	4.54	28.3	80.3	661	-541

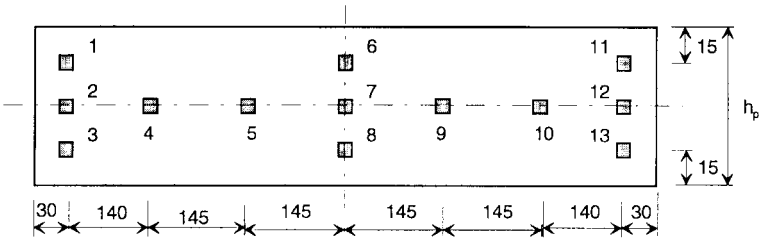

Fig. 7 Typical distribution of the strain gauges

3.2. Typical beam behaviour

The applied loads in Fig. 6(a) were gradually increased until the plates debonded. Debonding always occurred well within the flexural capacity of the reinforced concrete beam. The initial crack formation for a beam with a 60 mm deep plate is shown in Fig. 8 where the number next to a crack is the applied load P at which the crack formed. It can be seen that a flexural crack first occurred in the unplated region at 20 kN after which the first or initial debonding crack occurred adjacent to the plate-end at 45 kN and then propagated at 51 kN. These debonding cracks then spread around the plate-end as shown in Fig. 9.

The results from Beam 1aN are given in Table 2. The strain gauges in Fig. 7 are listed in column (1) in Table 2 and they have been grouped in column (2) according to their longitudinal position. The loads in column (3) are the applied loads at which the strains in the corresponding gauge reduced having reached their maximum values listed in column (4); this was interpreted as the load at which debonding had occurred in the region adjacent to the strain gauge. The corresponding debonding moments are given in column (5).

On loading, the strains at a plate-end became tensile as shown by the results of strain-gauge No.2 in Fig. 10 and on debonding at very low strains, at the load level at A, the strains became compressive indicating some form of residual stress was present. The rate at which debonding occurred along the length of a plate can be seen by comparing the results from the horizontal line of strain gauges 2, 4, 5 and 7 in Fig. 7, which are shown in Fig. 10. At the plate-end, gauge 2 indicated debonded at 30 kN at point A, the next gauge at 71 kN at point B, and then gauges 5 and 6 debonded simultaneously at 81 kN at point C. This would suggest that even though debonding started at a very low load, it stabilised until there was very rapid crack propagation at the maximum

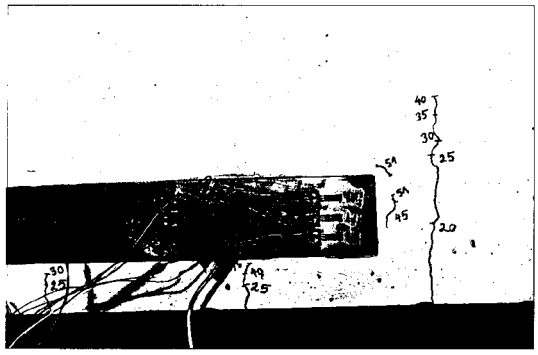

Fig. 8 Initial crack formation around a plate

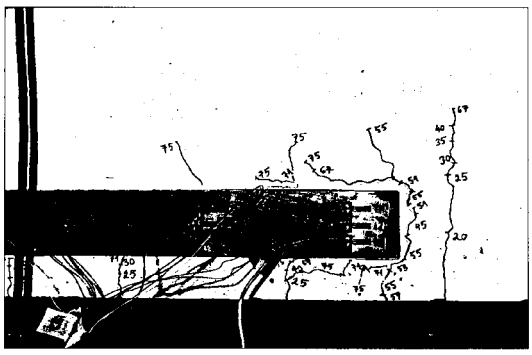

Fig. 9 Debonding crack formation

Table 2 Beam 1aN-Test results at debonding

Strain-gauge Level & No. (1)	Strain-gauge Position Group (2)	Total Applied Load P (kN) (3)	Maximum Strain (micro-strain) (4)	Moment (kNm) (5)
Top (No. 1)		29.7	25	22.3
Middle (No. 2)	Plate End	29.7	45	22.3
Bottom (No. 3)		24.0	61	18.0
Middle (No. 4)	Intermediate	71.3	253	53.5
Middle (No. 5)		81.3	474	61.0
Top (No. 6)		81.3	400	61.0
Middle (No. 7)	Centre	81.3	490	61.0
Bottom (No. 8)		81.3	570	61.0
Middle (No. 9)	Intermediate	65.3	398	49.0
Middle (No. 10)		62.9	259	47.2
Top (No. 11)		29.7	40	22.3
Middle (No. 12)	Plate End	29.7	47	22.3
Bottom (No. 13)		29.7	52	22.3

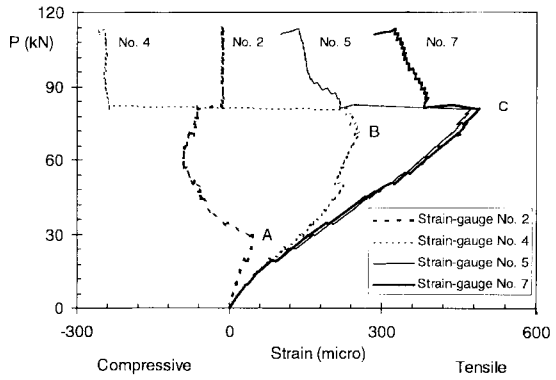

Fig. 10 Rate of debonding of plate

peeling moment. The strain gauges at the centre of the plate debonded simultaneously at 61 kNm as shown in column (5) in Table 2; the corresponding strains at the top and bottom levels in column (4) are given in columns (8) and (9) in Table 1 where tensile strains are positive.

3.3. Results

The results of the beam tests are given in Table 1. The initial peeling momentM_i in column (6) is the moment at which the first plate-end debonded. The ultimate peeling momentM_u is the moment at which the centre of the plate debonded and the ultimate strainsε_u in columns (8) and (9) are the strains at which debonding occurred at the bottom and top strain gauges at the centre of the plate. It can be seen that the range of strains in the plate at which the ultimate debonding occurred is very large and, therefore, cannot be used to control debonding.

The variation in the flexural peeling resistance with plate thickness is shown in Fig. 11 where the

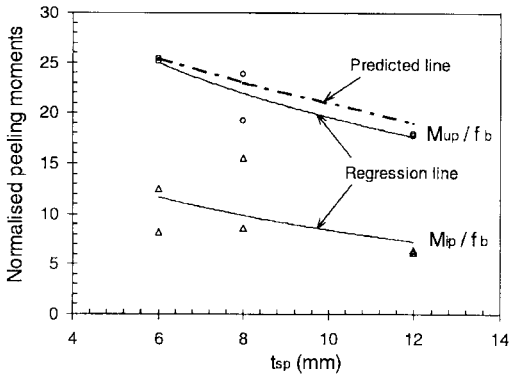

Fig. 11 Variation in plate thickness

normalised peeling moment is the debonding moment divided by f_b. It can be seen that the initial peeling moment M_i occurs at a much lower moment than ultimate peeling M_u and, therefore, initial peeling or the start of the peeling crack may occur at serviceability loads. It is also worth noting from the tests that the resistance to peeling increases with the plate depth which will encourage the use of deep plates.

4. Design rules for flexural peeling

4.1. Calibration of flexural peeling model

The twelve beam test results have been used to derive the constants k_A and k_B in Eq. (14). In deriving the fundamental parameters X and Y, the experimental ultimate peeling moment M_u was used for M_{cmp}, the Brazilian tensile strength f_b for the concrete tensile strength f_t, and the flexural rigidity $(EI)_{cmp}$ was derived from the flexural rigidity of the cracked plated beam which was calculated by assuming the tensile strength of the concrete was zero and using the Young's moduli in Table 1. The results are plotted in Fig. 12 and a linear regression analysis of the data through the mean (Nguyen and Oehlers 1997c) gave the intercept $k_{A,mn}$=0.0185, slope k_B=0.185 and a standard deviation of 0.0059. It is worth noting that an analysis using the uncracked plated properties gave a

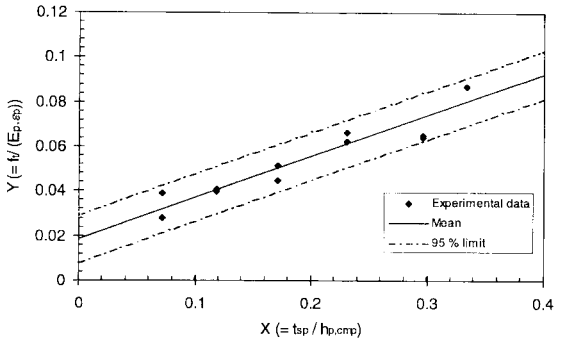

Fig. 12 Calibration of mathematical model

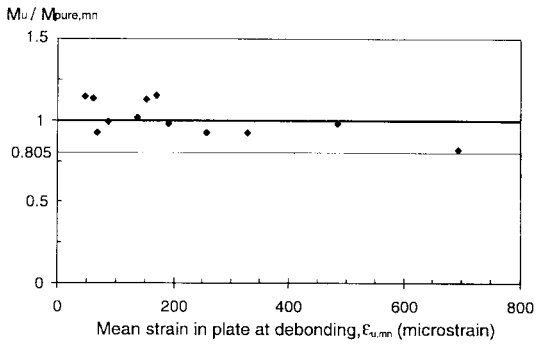

Fig. 13 Mean strain in plate at debonding

standard deviation of 0.0104 which is almost double that from the cracked section. Substituting these values of k_A and k_B into Eq. (14) gives the following mean peeling strength when the plate-end is subjected to pure flexure

$$M_{pure,mn}=\frac{f_b(EI)_{cmp}}{E_p(0.0185h_{p,cmp}+0.185t_{sp})} \tag{17}$$

The predicted flexural peeling strengths, $M_{pure,mn}$ from Eq. (17), are compared with the experimental variation with t_{sp} in Fig. 11 and in Fig. 13 with the experimental strengths M_u. As would be expected in the latter, the mean is 1 as the same experimental results were used to calibrate the mathematical model. However, it is worth noting that the scatter is fairly small even though a wide range of plate thicknesses, from 6 to 12 mm, and a wide range of plate depths, from 60 to 240 mm, had been used. It is also worth noting that the prediction equation has been validated over a very wide range of plate strains at debonding, as $47\times 10^{-6} < \varepsilon_p < 695 \times 10^{-6}$ and $-790 < \varepsilon_u < 1183 \times 10^{-6}$. The lower 95% confidence limit occurs at a standard deviation of 0.108 and, hence, for the eleven degrees of freedom the lower confidence limit occurs at 0.805. Therefore, the characteristic peeling strength is

$$M_{pure,ch}=0.805M_{pure,mn}=\frac{0.805f_b(EI)_{cmp}}{E_p(0.0185h_{p,cmp}+0.185t_{sp})} \tag{18}$$

In order to ensure that the design rules are applied within the range of the experimental data from which they were calibrated it is necessary to ensure that the centroid of the plate is in the tensile region of the composite plated beam and that

$$0.09d \leq h_{p,cmp} \leq 0.43d \tag{19}$$

where d = effective depth of the reinforced concrete element as shown in Fig. 2(a).

5. Conclusions

The fundamental parameters that control the flexural peeling of side plated reinforced concrete beams have been determined and calibrated experimentally. In the companion paper, the effect of shear on flexural peeling is quantified to produce design rules that can be used to prevent premature debonding of adhesive bonded steel side plates.

Acknowledgements

This work forms part of an ongoing research project between the Universities of New South Wales and Adelaide that is funded by a Large Australian Research Council Grant.

References

Nguyen, N.T. and Oehlers, D.J. (1997a), "A mathematical model for flexural peeling of side-plated glued beams", Dept. of Civil and Environmental Engng., University of Adelaide, Research Report R 143, Feb.

Nguyen, N.T. and Oehlers, D.J. (1997b), "Experimental investigation of flexural peeling of glued side-plated beams". Dept. of Civil and Environmental Engng., University of Adelaide, Research Report R 141, Feb.
Nguyen, N.T. and Oehlers, D.J. (1997c), "Interaction curves for flexural and shear peeling of side-plated glued beams". Dept. of Civil and Environmental Engng., University of Adelaide, Research Report R 152, April.
Oehlers, D.J. and Moran, J.P. (1990), "Premature failure of externally plated reinforced concrete beams". *Journal of Structural Engineering, ASCE*, **116**(4), 978-995, April.
Oehlers, D.J. (1992), "Reinforced concrete beams with plates glued to their soffits", *Journal of Structural Engineering, ASCE*, **118**(8), Aug. 2023-2038.
Oehlers, D.J. (1995), "Rules for bonding steel plates to existing reinforced concrete slabs", *Australian Civil Engineering Transactions*, **CE37**(1), Feb., 15-20.
Oehlers, D.J., Mohamed Ali, M.S. and Lou, W. (1998a), "Upgrading continuous reinforced concrete beams by gluing steel plates to their tension faces". *Journal of Structural Engineering, ASCE,* Mar., **124**(3).
Oehlers, D.J., Nguyen, N.T. and Bradford, M.A. (2000). "Retrofitting by adhesive bonding steel plates to the sides of R.C. beams", *Structural Engineering and Mechanics, An Int'l Journal*, **9**(5).
Ryder, G.H. (1974), *Strength of Materials*, Macmillan, London.
Smith, S.T. and Bradford, M.A. (1995), "Ductility of reinforced concrete beams with side and soffit plates", *Proceedings of the 14th Australasian Conference on the Mechanics of Structures and Materials* , University of Tasmania, Hobart, Australia, Dec.
Swamy, R.N., Jones, R. and Bloxham, J.W. (1987), "Structural behaviour of reinforced concrete beams strengthened by epoxy-bonded steel plates", *The Structural Engineer*, **65A**(2), Feb., pp59-68.

Notations

A_p = cross-sectional area of a plate; $h_p t_{sp}$
b_c = width of reinforced concrete beam
d = effective depth of reinforced concrete element; distance from compression face to centroid of tensile reinforcing bars
E = Young's modulus
E_c = short term Young's modulus of concrete at time of testing
E_p = Young's modulus of plate
$(EA)_p$ = axial rigidity of a plate
$(EI)_{cmp}$ = flexural rigidity of composite plated beam; flexural rigidity of cracked plated section
$(EI)_p$ = flexural rigidity of a plate element
$(EI)_{RC}$ = flexural rigidity of reinforced concrete element
F_a = normal force across interface
F_p = axial force induced in a plate
f_a^t = maximum normal tensile stress induced by F_p
f_b = Brazilian tensile strength
f_c = compressive cylinder strength of concrete
f_F = normal tensile stress across interface induced by F_p
f_P = mean tensile stress induced by F_p
f_t = tensile strength of concrete
h = distance from centre of transmission zone
h_p = depth of plate
$h_{p,cmp}$ = distance between neutral axis of composite plated beam and centroid of plate
$h_{p,RC}$ = distance between the centroid of the plate and the centroid of the reinforced concrete element
I = second moment of area about centroid
I_p = second moment of area of plate about its centroid
k = constant
M_{cmp} = moment applied to composite plated beam
M_i = experimentally determined initial peeling moment

M_p = moment induced in plate acting at the centroid of the plate
$M_{pure,mn}$ = mean pure flexural peeling resistance
M_{RC} = moment induced in reinforced concrete element at the centroid of the reinforced concrete element
M_u = experimentally determined ultimate peeling moment
N = north plate
P = total load applied to beam
S = south plate
s_a = shape factor for normal tensile stress distribution
t_{sp} = thickness of side plate
X = debonding parameter; $t_{sp}/h_{p,cmp}$
Y = debonding parameter; $f_t/E_p\varepsilon_p$
ε = strain; strain profile
ε_p = strain at centroid of plate
ε_u = strain at the centre of the plate at which debonding occurred
$\varepsilon_{u,mn}$ = mean strain at centre section at debonding
ϕ = curvature
τ_F = shear stress induced by F_p
τ_h = shear stress at distance h from centre of transmission zone
τ_M = shear stress induced by M_p
$\tau_{\max}$ = maximum shear stress induced by M_p; shear stress at the circumference of the transmission zone, that is at $h=h_p/2$
τ_{sh} = shear stress induced by F_p